INTERNATIONAL JOURNAL FOR NUMERICAL METHODS IN FLUIDS
Int. J. Numer. Meth. Fluids **30**: 743–761 (1999)

EFFECTS OF REYNOLDS NUMBER ON PHYSIOLOGICAL-TYPE PULSATILE FLOWS IN A PIPE WITH RING-TYPE CONSTRICTIONS

T.S. LEE* AND Z.D. SHI

Mechanical and Production Engineering Department, National University of Singapore, 10 Kent Ridge Crescent, Singapore 119260, Singapore

SUMMARY

The effects of Reynolds number on the physiological-type of laminar pulsatile flow fields within the vicinity of mechanical ring-type constriction in small pipes were studied numerically. The parameters considered are: the Reynolds number (Re) in the range of 50–1500; Strouhal number (St) in the range of 0.00156–3.98; Womersley number (Nw) from 0.0 to 50.0. The pulsatile flows considered were physiological-type of simulated flows. Within a pulsating cycle, detailed flow characteristics were studied through the pulsating contours of streamline (ψ), vorticity (Ω), shear stress (τ) and isobar. The relations between the instantaneous flow rate (Q) and instantaneous pressure gradients ($\mathrm{d}p/\mathrm{d}z$) are observed to be elliptic. The relations between the instantaneous flow rate (Q) and pressure loss (P_{loss}) are quadratic. Linear relations were observed between the instantaneous flow rate (Q) and the maximum velocity, maximum vorticity and maximum shear stress. The Reynolds number of the flow in a pulsating cycle was found to have significant effects on the recirculation length and the pressure gradient within the pulsatile flow regime. Copyright © 1999 John Wiley & Sons, Ltd.

KEY WORDS: pulsatile flow; ring-type constrictions; numerical experimentation

1. INTRODUCTION

In recent years, pulsatile flows have attracted increased attention due to their uses in the big engineering related fields. In the study of intracardiac flow and stenosis in blood vessel, the pressure loss, the maximum flow velocity, shear stress and the recirculation region are parameters of extreme interest because of their relationship with the atheroma caused by the large pressure drop across the constriction created through artificial implants, the corpuscle damage by large shear stress, as well as the thrombus phenomena resulted from the recirculation region [1–7]. However, most of the above studies are for 'smooth' sinusoidal profiles or bell shape constrictions [1,2,8,9]. Few considered ring-type constrictions with sharp edges. An investigation is carried out here to study the effects of the Reynolds number on the physiological-type of unsteady flow fields in the vicinity of ring-type constrictions. Unsteady flow through ring-type constrictions are of interest to the designer of unsteady flow measuring

* Correspondence to: Mechanical and Production Engineering Department, National University of Singapore, 10 Kent Ridge Crescent, Singapore 119260, Singapore.

Contract/grant sponsor: National University of Singapore; Contract/grant number: RP0633

CCC 0271–2091/99/140743–19$17.50

Received September 1997
Revised August 1998

devices [8]. The relationship between flow rate and pressure loss across the ring-type constrictions provides a mean of estimating the mean flow rate from the measured pressure loss. Hence, unsteady flow through ring-type constriction is used here as a model for the study of the application of fluid devices implant in intracardiac flow. A physiological flow and two experimentally approximated physiological pulsatile flow in a rigid pipe with a ring-type constriction were selected in the present numerical study. The present investigation focused on the variation of the pressure gradient along the axial direction, the pressure loss in flow passing through the constriction, the maximum flow velocity, maximum vorticity and maximum shear stress, the recirculation length, as well as the centreline velocity profiles in the developing flow. The results of the ring-type constriction presented here are for $d/D = 0.5$ opening ratio and $h/D = 0.1$ thickness ratio. The mean flow Reynolds number is of the order 50–1500. The flow Strouhal numbers (St) considered are in the range 0.00156–3.98 with the corresponding Womersley number (Nw) ranges from 0.0 to 50.0. In the vicinity of the implanted solid rigid-type constriction, the tube wall can be considered as relatively rigid. Hence, a rigid tube assumption is made in this study.

2. GOVERNING EQUATIONS AND NUMERICAL PROCEDURES

The dimensionless governing equations for the axisymmetry unsteady incompressible laminar flow through the ring-type constriction, as shown in Figure 1(a), are given by

Continuity equation:

$$\frac{\partial}{\partial z}(ru) + \frac{\partial}{\partial r}(rv) = 0; \tag{1}$$

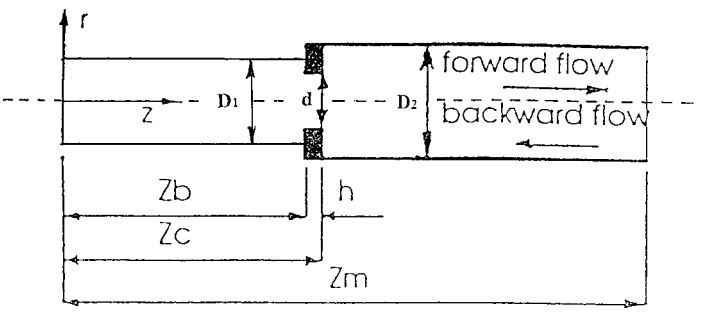

(a) co-ordinate system and geometrical parameters

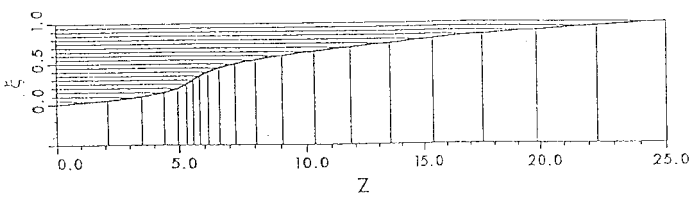

(b) grid distribution in z-direction

Figure 1. pipe with ring-type constriction.

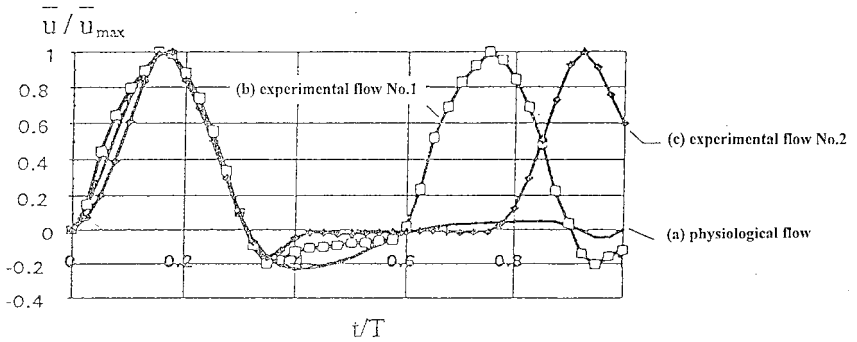

Figure 2. Three types of pulsatile flow.

z-Direction momentum equation:

$$St\frac{\partial u}{\partial t}+\frac{\partial}{\partial z}(u^2)+\frac{1}{r}\frac{\partial}{\partial r}(ruv)=-\frac{\partial p}{\partial z}+\frac{\partial}{\partial z}\left(\frac{2}{Re}\frac{\partial u}{\partial z}\right)+\frac{1}{r}\frac{\partial}{\partial r}\left[\frac{r}{Re}\left(\frac{\partial u}{\partial r}+\frac{\partial v}{\partial z}\right)\right]; \tag{2}$$

r-Direction momentum equation:

$$St\frac{\partial v}{\partial t}+\frac{\partial}{\partial z}(uv)+\frac{1}{r}\frac{\partial}{\partial r}(rv^2)=-\frac{\partial p}{\partial r}+\frac{\partial}{\partial z}\left[\frac{r}{Re}\left(\frac{\partial v}{\partial z}+\frac{\partial u}{\partial r}\right)\right]+\frac{1}{r}\frac{\partial}{\partial r}\left(\frac{2}{Re}\frac{\partial u}{\partial r}\right)-\frac{1}{Re}\frac{2v}{r^2}. \tag{3}$$

In the solution domain, as shown in Figure 1(a), the upstream inlet velocity conditions are specified by one of the pulsatile flows [10–12], as shown in Figure 2. At each time step, along the solid wall, a no-slip velocity condition is specified by $u=0$, $v=0$. Along the central line, axisymmetric conditions are applied to all variables with $\partial u/\partial r=0$, $v=0$, $\partial p/\partial r=0$. At the downstream exit section, the dimensionless pressure is fixed at zero and the flow is considered to be fully developed, so $p=0.0$, $\partial u/\partial z=0$ and $\partial v/\partial z=0$.

In a general curvature co-ordinate system (ξ, η), Equations (1)–(3) can be expressed as:

$$\frac{\partial G}{\partial t}+\frac{\partial}{\partial \xi}(E-M)+\frac{\partial}{\partial \eta}(F-N)-S=0, \tag{4}$$

where

$$\xi=\xi(z, r), \qquad \eta=\eta(z, r). \tag{5}$$

The variables (G, E, M, F, N, S) are functions of physical variables (u, v, p) and the geometrical variables (z, r). They are expressed in details by Jones and Bajura [8] and Marcelo *et al.* [13] and will not be repeated here.

The curvilinear velocity components U, V in Equation (4) are related to the Cartesian velocity components u, v in Equations (1)–(3) by

$$\begin{aligned} U&=u\xi_z+v\xi_r \\ V&=u\eta_z+v\eta_r \end{aligned}. \tag{6}$$

The time-dependent term in Equation (4) can be expressed as [1,2]

$$G=\frac{1}{2\pi}\frac{(Nw)^2}{Re}\cdot Jr(0, u, v)^T \tag{7}$$

and the Womersley number (Nw) is then considered as a characteristic non-dimensional parameter of unsteady flow. The relation between the Strouhal number (St) and the Womersley number (Nw) is $\sqrt{2\pi\, Re \cdot St}$.

Equation (4) is then solved by an iterative process. All the physical variables (u, v, p) are updated through

$$\phi^{n+1} = \phi^n + \delta\phi, \tag{8}$$

where n and $(n+1)$ are the last and current iteration numbers, and ϕ represents each of the physical variables. Substituting Equation (8) into Equation (4), the governing equations can be expressed in incremental form of

$$\frac{\partial \delta F}{\partial t} + \frac{\partial}{\partial \xi}(\delta E - \delta M) + \frac{\partial}{\partial \eta}(\delta F - \delta N) - \delta S = -R. \tag{9a}$$

The residual vector, R, is calculated by using the variable's value at level n as

$$R = \frac{\partial G^n}{\partial t} + \frac{\partial}{\partial \xi}(E - M)^n + \frac{\partial}{\partial \eta}(F - N)^n - S^n. \tag{9b}$$

Equations (9a) and (9b) are solved by the SIMPLE algorithm [14] on a non-staggered grid. The grid point distribution within the solution domain is shown in Figure 1(b). A stretching function is used along the axial direction:

$$\frac{\mathrm{d}z}{\mathrm{d}\xi} = z_{\mathrm{m}}[\alpha + \beta(\xi - \xi_1)^2 \gamma^{\xi}], \tag{10a}$$

with the boundary conditions given by:

$$z\big|_{\xi=0} = 0, \qquad z\big|_{\xi=1} = z_{\mathrm{m}} \tag{10b}$$

where z_{m} is the maximum length of the solution domain in the axial direction. α and γ are two grid controlling parameters. At point $\xi = \xi_1$, the grid size is $\Delta z = z_{\mathrm{m}} \alpha\, \Delta\xi$, which can be controlled through the value of α. If $\alpha < 1.0$, the grid will become more clustered at point $\xi = \xi_1$. The grid distribution for the z-direction can be further refined through the parameter γ.

With the grid distribution as defined by Equation (10), all terms containing the incremental variables ($\delta E, \delta M, \delta F, \delta N, \delta S$) are discretized by three-point difference schemes. The hybrid difference schemes are used for convective terms, the second-order central schemes for diffusive terms, the first-order forward schemes for pressure terms and backward schemes for continuity equation. The residual vector is calculated by the second-order difference schemes, which are the second-order upwind scheme for convective terms, the central schemes for diffusive terms, the second-order forward schemes for the pressure terms and the second-order backward schemes for the continuity equations. At convergence, the residual vector (R) is equal to zero, and the convergent results have the second-order accuracy. For points adjacent to the wall, the corresponding second-order difference schemes are also used to ensure the consistency of the scheme accuracy.

For the time-dependent terms, a modified Crank–Nicolson scheme is used to discretize the governing equations:

$$\frac{\delta G^{n+1} - \delta G^n}{\Delta t} + \theta \cdot X^{n+1} + (1-\theta) \cdot X^n = -R, \tag{11}$$

where $X = (\partial/\partial\xi)(\delta E - \delta M) + (\partial/\partial\eta)(\delta F - \delta N) - \delta S$ and θ is a scheme controlling parameter ranges from 0.0 to 1.0. $\theta = 0.0$ is for the time explicit scheme, $\theta = 1.0$ is for the time implicit scheme, and $\theta = 0.5$ is for the standard Crank–Nicolson scheme. The optimum θ value in the present numerical computation is determined from numerical experiment to obtain stable and convergent results. In the present work, $\theta = 0.6$ is chosen after a series of numerical experimentations. Second-order discretization of pressure gradient terms and the continuity equations are adjusted according to the instantaneous main flow direction. This numerical scheme was found to be most accurate and numerically stable for the pulsatile flow problems studied here.

The numerical procedure for the pulsatile flow computation adopted in this study can be briefly outlined as follows:

1. Steady flow is computed and taken as initial conditions for the unsteady flow computation. At the advancement of each time step, initial velocity and pressure fields are given by the converged values of last time step, and boundary values of each variable are specified.
2. The momentum equations are solved by sweeping in the positive and negative redirection with an underrelaxation procedure. The underrelaxation factor is 0.35. The residual of each equation is computed. Iteration continued until the residuals of all the equations reduce to 0.1% of their values at the first iteration.
3. The residual of continuity equation is computed and used as the source terms of the pressure correction equation, which is then solved by the ADI sweeps. The sweep is repeated until the residual of pressure correction equation reduces to 0.1% of its value at the first iteration.
4. The flow flux at each section in the z-direction is computed. The maximum equation residual and maximum flux difference to that at inlet section are obtained. The program will return to step (2) when the maximum residual or maximum flux difference is greater than 0.1% of the initial values.
5. At convergence, the streamline, vorticity, shear stress fields are computed from the velocity field. Information about pressure is obtained from pressure field.

3. RESULTS AND DISCUSSIONS

For the computation of flow field in the pipe with a ring-type constriction, non-uniform grids were used in the axial z-direction with more grid points being distributed nearer the constriction as shown in Figure 1(b). For the radial direction and the time domain, computational grids were evenly distributed. Grids with 15, 21, 31 points in the r-direction and 81, 101, 121, 141 points in the z-direction were tested. Grids with 31, 41 and 51 points per pulsatile period (T) in the time domain were tested for the first three time periods to check on the grid point independency on the numerical results obtained. Further computations are then based on a grid point arrangement of 21, 121, 41 in the r-, z- and t-directions respectively. Monotonic convergence towards a grid-independent value is also found for all the solutions obtained here. An estimation of the grid-independent values is made by applying the Richardson extrapolation. Assuming second-order behaviour, the 'exact' values of the solution field are obtained from $\Phi = \Phi_h + [\Phi_h - \Phi_{2h}]h/3$. Where '$h$' here denotes the uniform mesh size $\Delta\zeta$ used within the transformed domain for the z-direction. Since the convergence errors were kept below 0.01% in the present solutions, the results of the above extrapolation are assumed to have errors an order of magnitude lower than the finest grid used in the solution. Computations were carried out for more than one periodical time cycle for every pulsatile unsteady flow conditions considered.

The validity of the numerical procedures and grid size were first verified against available data for steady laminar flow in two dimensional symmetric sudden expansion and axisymmetric sudden expansion in pipe. For the two-dimensional symmetric expansion flow, Kwon [15] investigated cases of $Re < 700$, by using 80×32 equally distributed grid points in the x- and

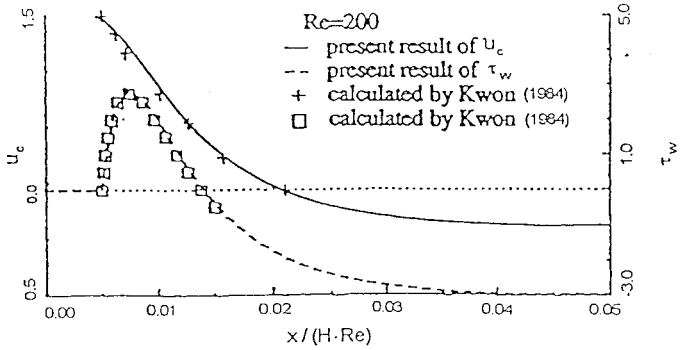

(a) centre-line velocity and wall shear stress of two-dimensional symmetric sudden expansion (h:H=1:2)

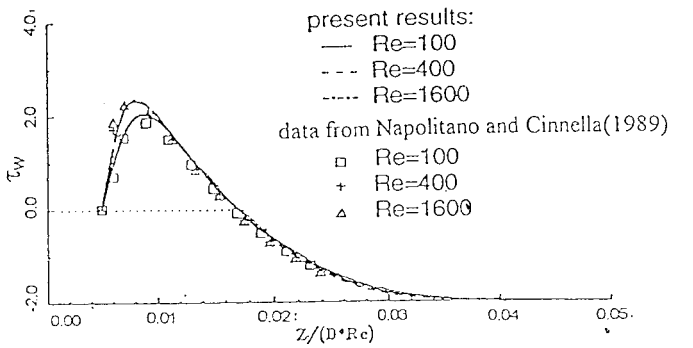

(b) wall shear stress of axisymmetric sudden expansion (d:D=1:2)

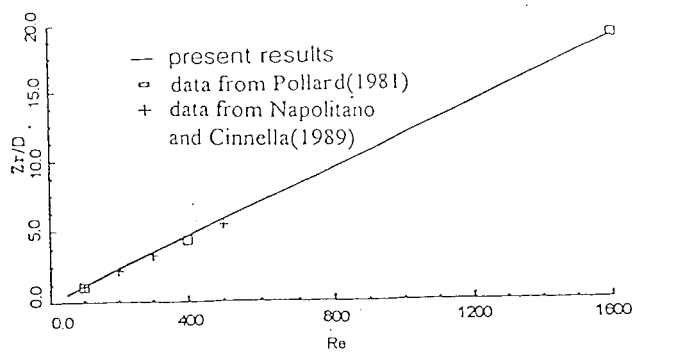

(c) recirculation length of axisymmetric sudden expansion (d:D=1:2)

Figure 3. Comparison of results with other investigators.

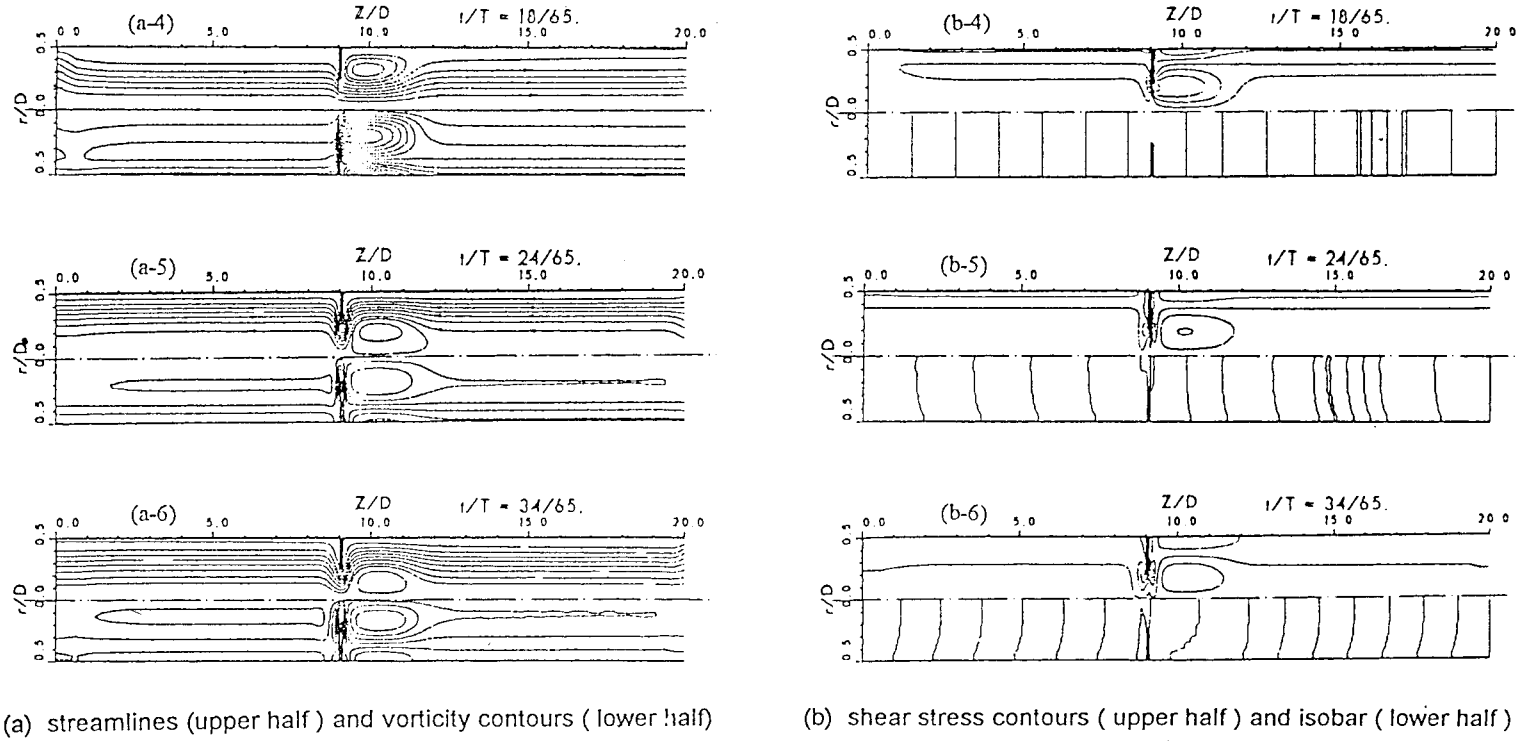

Figure 4. (a) and (b) Development of laminar pulsatile flow field at $Re = 50$, $Nw = 6.98$ and $St = 0.155$. (c) and (d) Development of laminar pulsatile flow field at $Re = 50$, $Nw = 6.98$ and $St = 0.155$. (e) and (f) Development of laminar pulsatile flow field at $Re = 50$, $Nw = 6.98$ and $St = 0.155$.

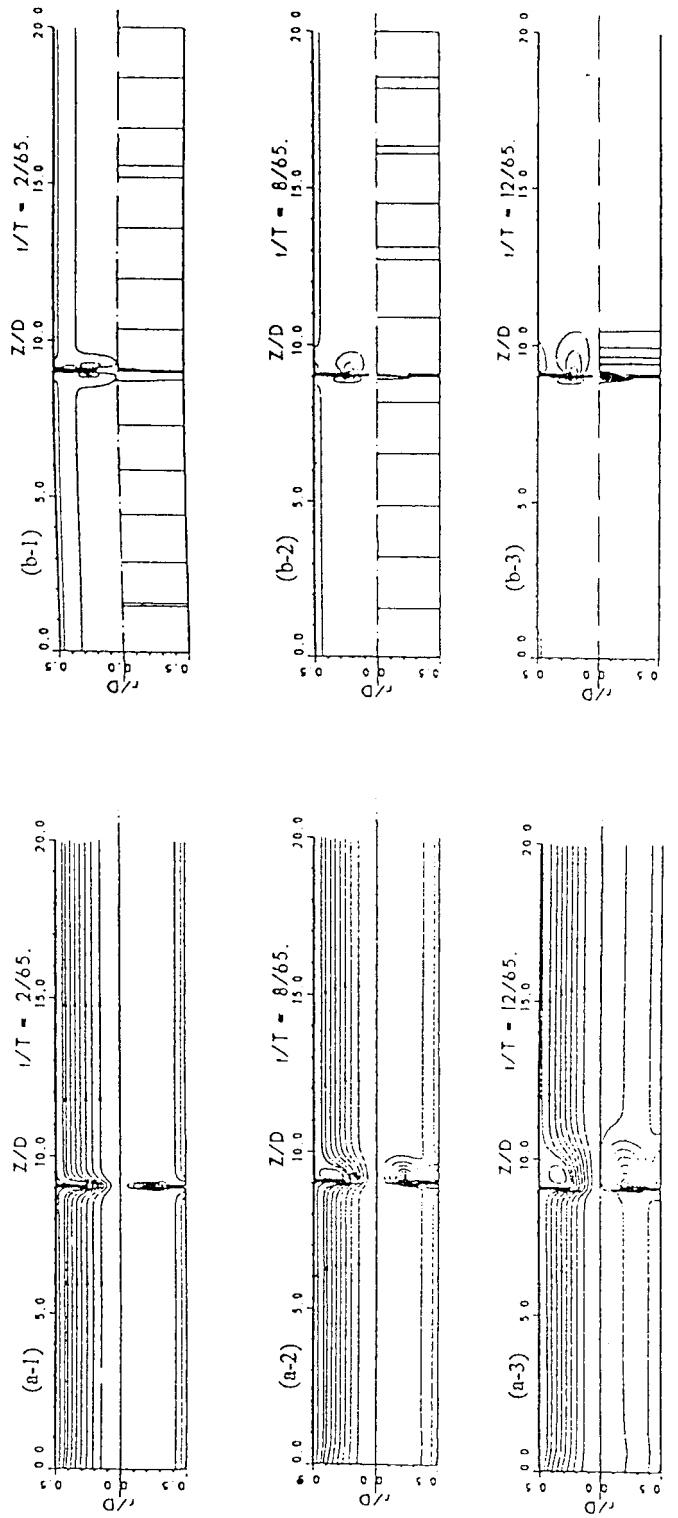

(c) streamlines (upper half) and vorticity contours (lower half)

(d) shear stress contours (upper half) and isobar (lower half)

Figure 4 (*Continued*)

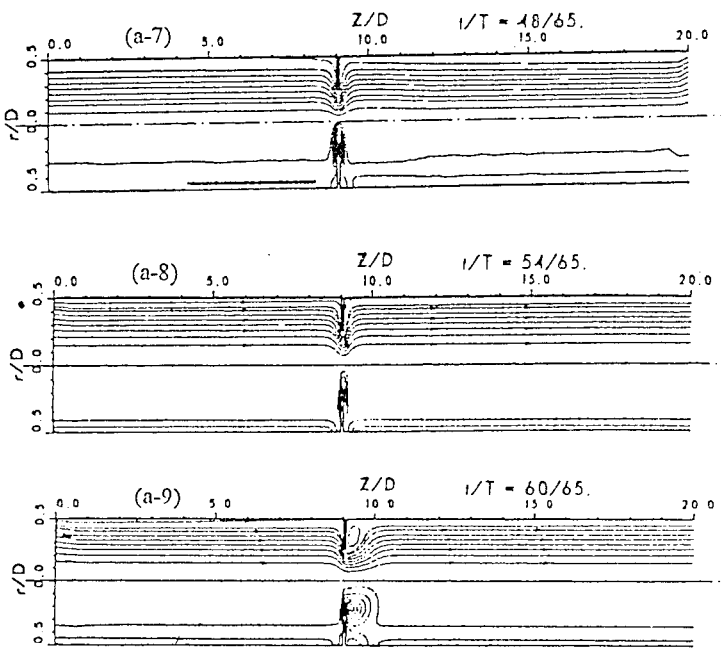

(e) streamlines (upper half) and vorticity contours (lower half)

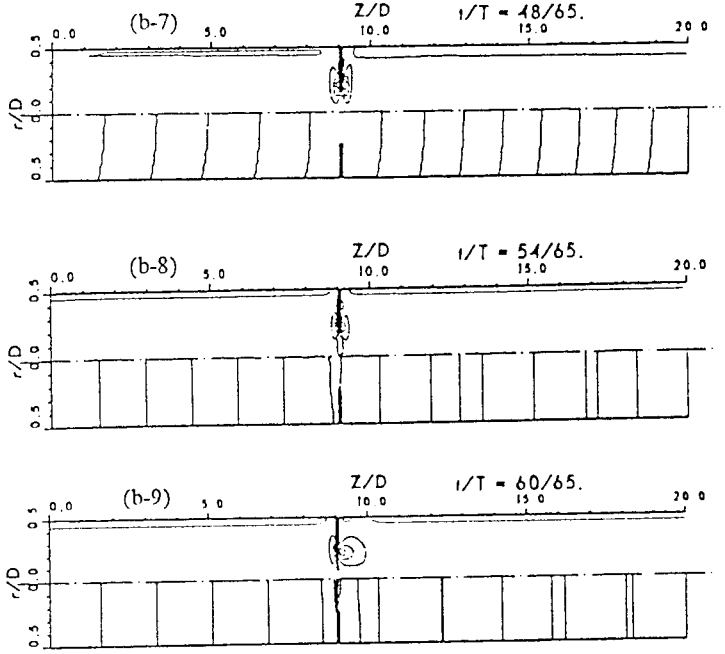

(f) shear stress contours (upper half) and isobar (lower half)

Figure 4 (*Continued*)

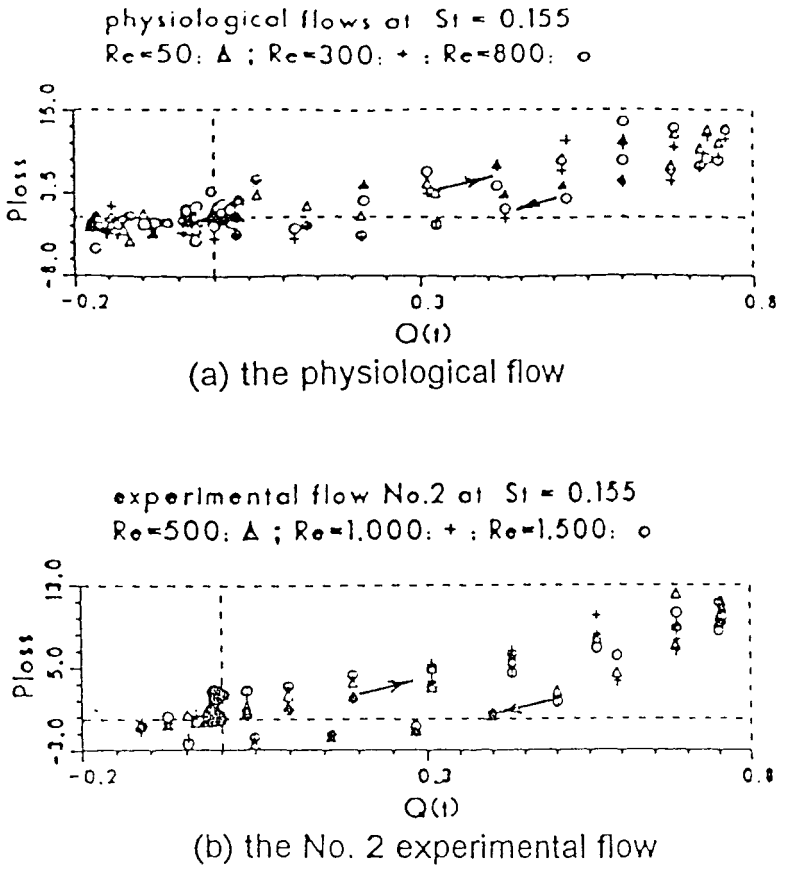

Figure 5. Relation between flow rate and pressure loss (arrows show direction of time increment).

y-directions. Comparison were made between the present results and data from Kwon [15] on the centreline velocity and wall friction distributions as shown in Figure 3(a). The computed results compared very well with the results obtained by Kwon [15]. Similar axisymmetric sudden expansion flow was studied by Napolitano and Cinnella [16] with the Block–Line–Gauss–Seidal method with 97×193 equally distributed grid points in the r- and z-directions. The flow Reynolds numbers were in the range of 100–1600. Pollard [17] also studied the axisymmetric sudden expansion flow for $Re < 100$ by using SIMPLE algorithm of Patankar with 28×57 non-uniform grids in both r- and z-directions. Similar test results were obtained in the present study and compared with data available from Pollard [17] and Napolitano and Cinnella [16] on the recirculation length and the wall shear stress. These are shown in Figure 3(b) and (c). The results show that the present numerical procedure and grid size used produce results that are accurate and consistent with the known steady laminar flow data. It is thus assumed here that similar procedure and grid size used for the pulsatile flow should also produce accurate results for the unsteady laminar flow cases to be considered here.

Following the studies by Coder and Buckley [18] and Durst *et al.* [19], the flow Reynolds number is known to have significant effects on the flow field for a given bell-shaped constriction opening. Investigations are then focused here on the effects of the Reynolds number on the flow field and the maximum values of velocity ($V_{\max}$), vorticity ($\Omega_{\max}$), shear

stress (τ_{max}), as well as the pressure loss (P_{loss}) across the ring-type constriction, the recirculation length (z_r/D). These parameters are of practical interest due to their relations with the big-mechanical study and the design of fluid devices implant in intracardiac flow. In the present study, the flow Reynolds number varies from 50 to 200. The opening ratio is fixed at 0.5 and thickness ratio fixed at 0.1. Three types of physiological-type pulsatile flow, as described in Figure 2, are computed with the flow Reynolds number in the range of 50–1500 for different Strouhal numbers and Womersley numbers.

The *typical pulsatile flow fields development* are shown in a series of time development flows in Figure 4. It shows the developments of the streamline field, the vorticity field, the distributions of shear stress and isobars. It should be noted here that when t/T advances from 0.0 to 10/65, forward flow is accelerated to the peak flow velocity. The recirculation length (z_r/D) increases from its steady flow value to a maximum value. As t/T further advances from 10/65 to 20/65, forward flow is decelerated back towards its minimum value and the z_r/D value decreases to its minimum value correspondingly. During t/T advances from 21/65 to 50/65, the flow is under small backward velocity period with $Q < 0.18$. At t/T varying from 50/65 to 1.0, the second cycle starts and the flow field repeats the same structure as previous cycle.

The above streamlines also show that the recirculation region in the unsteady flow domain is not stationary. For the duration where the instantaneous bulk velocity of the flow field is very small, the recirculation region in the flow domain is negligible. For the physiological-type of pulsatile flows investigated, flow acceleration and deceleration are of the same magnitude at the same instantaneous flow rate (Q). However, as shown in Figure 4, through the develop-

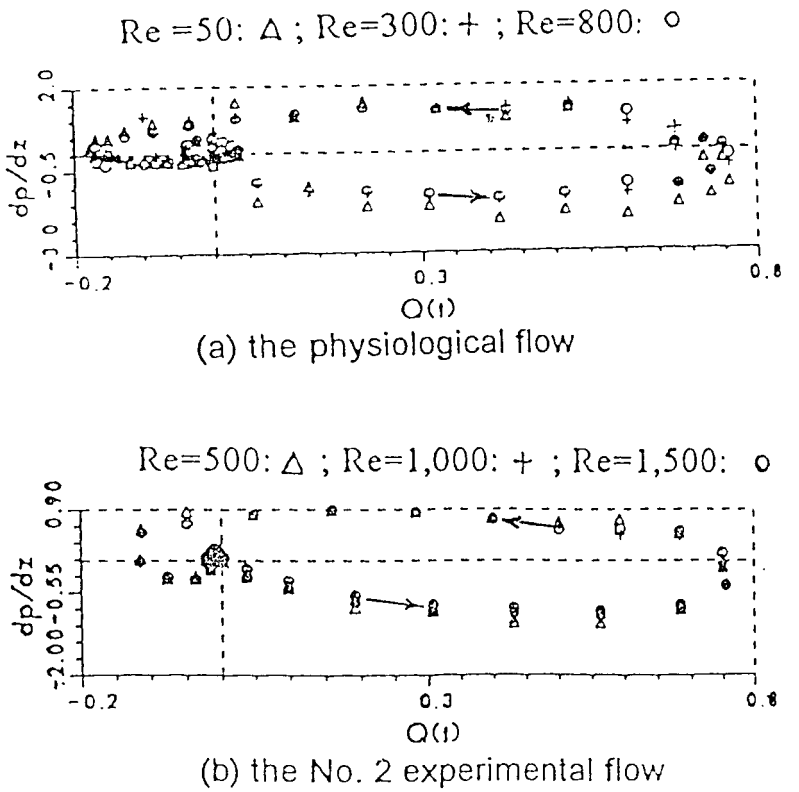

Figure 6. Relation between flow rate and axial pressure gradient (arrows show direction of time increment).

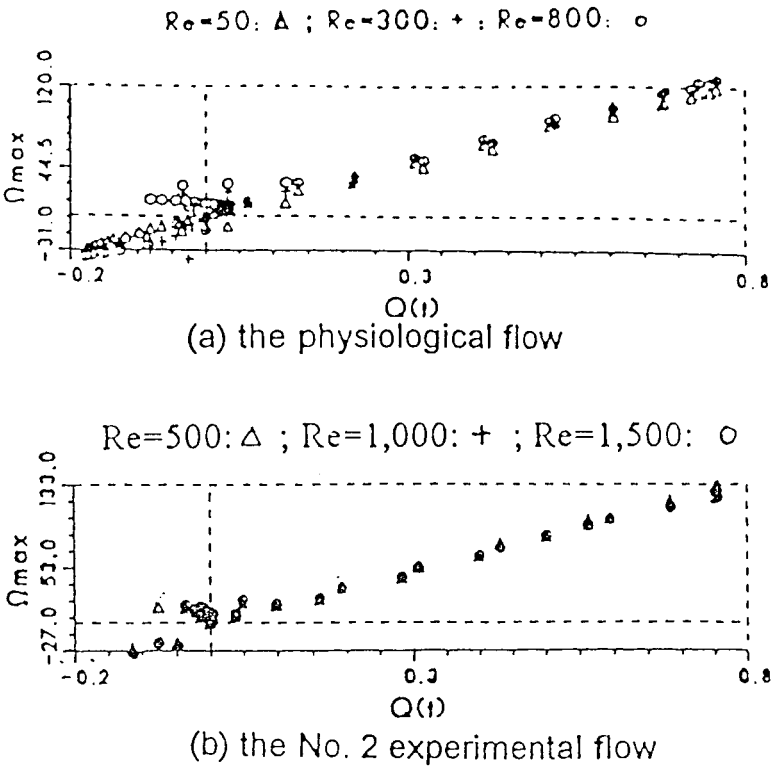

Figure 7. Relation between flow rate and maximum vorticity.

ment of the streamlines with the development of the recirculation region, it is noted that during the deceleration phases, the flow field results in larger recirculation length. The relationship between the maximum recirculation length and the Reynolds number is given by:

$$z_r/D + 0.0415Re.$$

However, in practice as $Re \to \infty$, the flow becomes turbulent. Hence, the above expression is only valid at low Reynolds number laminar flow. Figure 4 also shows that the maximum shear stress is located around the tip of constriction. In the region close to the constriction, the pressure, velocity have their large gradient in both r- and z-directions.

The relationship between *flow rate and pressure loss*, *axial pressure gradient* are non-linear. As shown in Figure 5, during the acceleration phases P_{loss} is larger when compared with the values of P_{loss} during the deceleration phases. The differences in the P_{loss} values can be as high as 3.0. One factor that causes this difference is the different magnitudes of acceleration and deceleration as shown by the characteristics of the pulsatile flows in Figure 2. The relationship between the flow rate and the axial pressure gradient in the fully developed flow region is presented in Figure 6 for the physiological flow at $Re = 50$, 300, 800 and for the pulsatile flow at $Re = 500$, 800 and 1500. It is noted that at the instant of maximum flow rate, the pressure gradient is small. The pressure gradient has its maximum value at the instant where the flow rate is approximately half of the maximum flow rate. The phase angle between the Q and dp/dz is about 80°.

Figure 7 shows the relationship between the *flow rate and the maximum vorticity*. The data on the physiological flow and the No. 2 experimental pulsatile flow can be approximated by a linear relationship of the form:

$$\Omega_{\max} = 170Q.$$

The above relationship remains unchanged for all the Reynolds numbers from 50 to 1500.

The numerical results on the maximum shear stress of the whole flow field are presented in Figure 8. The linear relationship can be expressed as an function of the form:

$$\tau_{\max} \cdot Re = 106Q.$$

The maximum wall shear stress ($\tau_{w,max}$) is not simply linked with the flow rate. This is shown in Figure 9. The $\tau_{w,max}$ value is about 1/4 of the τ_{max} value. Referring to Figure 4(b), the maximum shear stress occurs at the tip region of constriction, while the maximum wall shear stress is along the pipe wall. The flow field around the tip of the constriction is mainly determined by the constriction geometry. The flow structure adjacent to the wall depends on the recirculation size, the pulsatile Reynolds number that affects the instant velocity profiles as shown in Figure 4. Hence, the maximum wall shear stress is not related to the flow rate in a simple manner.

The *maximum velocity* of the whole flow field has different relationships with the flow rate for the acceleration and deceleration period, as shown in Figure 10. The starting point for the

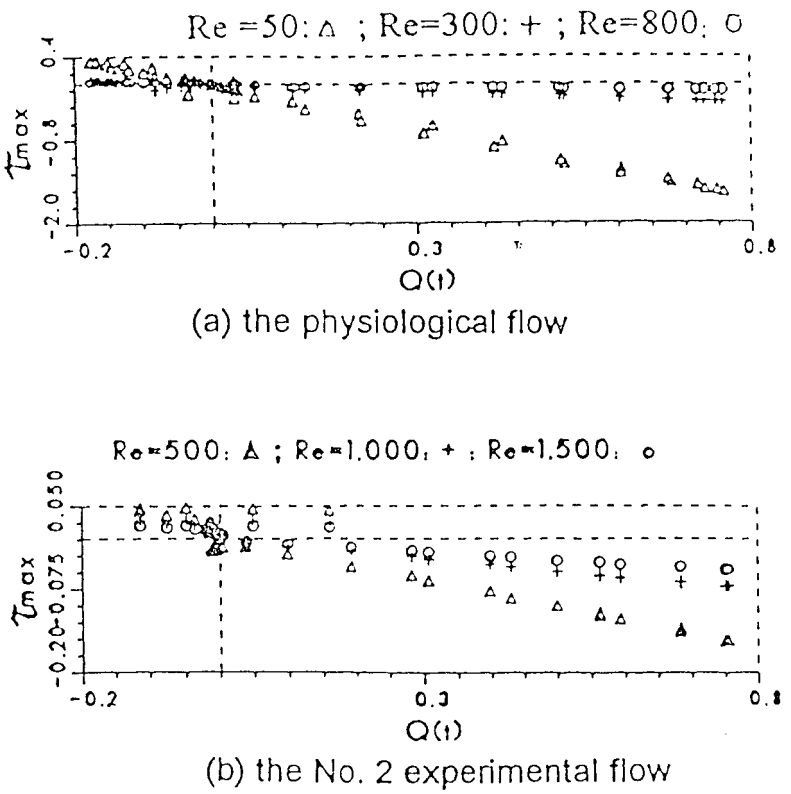

Figure 8. Relation between flow rate and maximum shear stress.

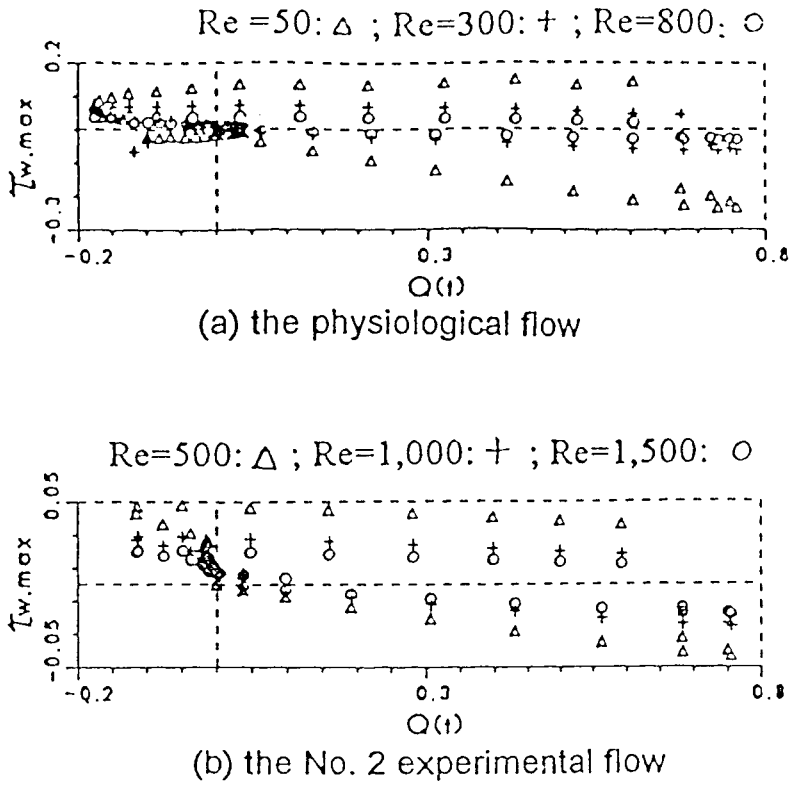

Figure 9. Relation between flow rate and maximum wall shear stress.

calculation is a stationary flow, i.e. $V_{\max} = 0.0$ at $t/T = 0.0$. The maximum velocity becomes large with the flow rate increase, and never equal to zero again. Approximately, the relationships can be expressed as:

$$V_{\max} = 7.32Q - 1.0 \quad \text{at acceleration}$$

and

$$V_{\max} = 3.82Q - 3.5 \quad \text{at deceleration.}$$

As shown in the velocity profiles of Figure 2, the flow is never stationary in the pipe even at the instantaneous $Q = 0.0$ for the pulsatile flow considered. The relation between the flow rate and maximum velocity is no longer linear.

At $Re = 50$ and 500, $St = 0.155$, comparisons among these three types of pulsatile flow are presented in Figures 11 and 12. Results of maximum values of shear stress, vorticity, velocity, and the recirculation length, pressure loss and axial pressure gradient are compared. These three types of laminar pulsatile flow have the same flow property. Hence, *in vitro* investigation of physiological laminar flow phenomena, the various types of experimental flow shown here are suitable for use in the investigations.

It is noted that in some of the cases considered above, the transient breakdown of laminar flow may appear, even though the maximum Reynolds number is below the critical value for steady flow. It depends on the frequency and velocity amplitude [20]. It is more pronounced in the case of flow in pipe with constriction. It is dependence on the constriction opening d/D

and the constriction thickness h/D. The present study used a Reynolds number $Re = 1500$ as the limiting cases but did not touch on the breakdown problems. Through a separate study by the authors with sinusoidal pulsatile flows [20], it was shown that for Reynolds number less than 1500, the flow characteristics is predominantly laminar in nature. Hence, transitional breakdown into turbulent flow can be neglected in the present study.

4. CONCLUSIONS

The effects of the flow Reynolds number in physiological-type pulsatile flow fields through a sharp edge ring-type constriction were investigated for flow Reynold number in the range of 50–1500, *Nw* from 0.0 to 50.0 and *St* from 0.0 to 3.98. *In vitro* investigation of physiological laminar flow phenomena through the ring-type constriction showed that the three types of experimental flows investigated here are suitable. Numerical experimentations show that flow deceleration in the pulsatile cycles tends to enlarge the recirculation region and its effect becomes more significant with the increase of the Reynolds number of the net forward flow of the physiological type of pulsatile flow. The corresponding flow acceleration in the pulsatile cycles tends to increase the pressure drop in the pipe flow. Other more specific flow characteristics are also observed. The relationship between the instantaneous flow rate and the pressure loss across the constriction is quadratic. However, the relationship between instantaneous flow rate and pressure gradient is elliptic. The time-averaged pressure gradient along the axial direction trend towards a stationary value when the flow is increase to the maximum

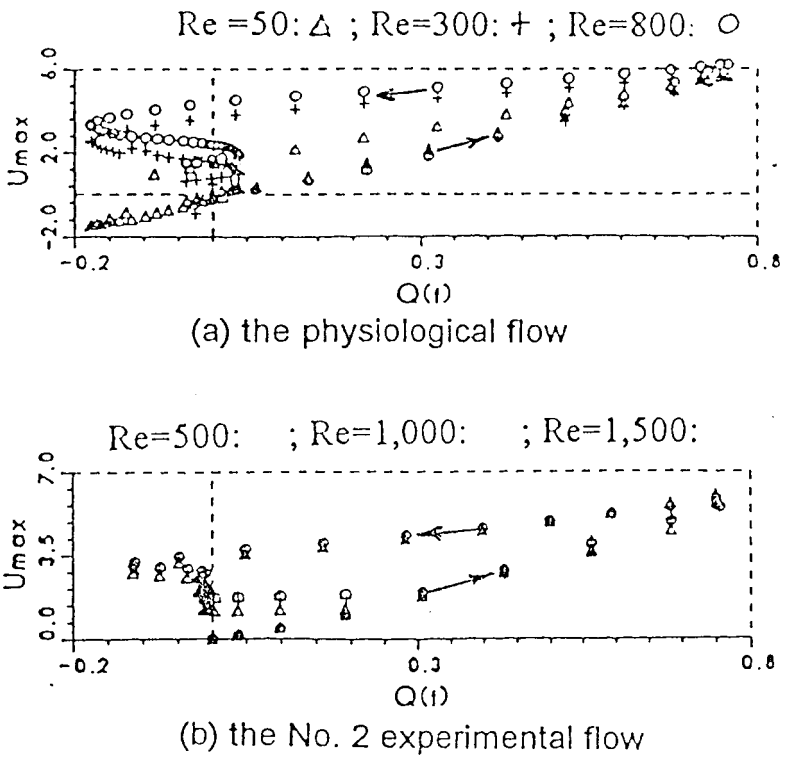

Figure 10. Relation between flow rate and maximum velocity (arrows show direction of time increment).

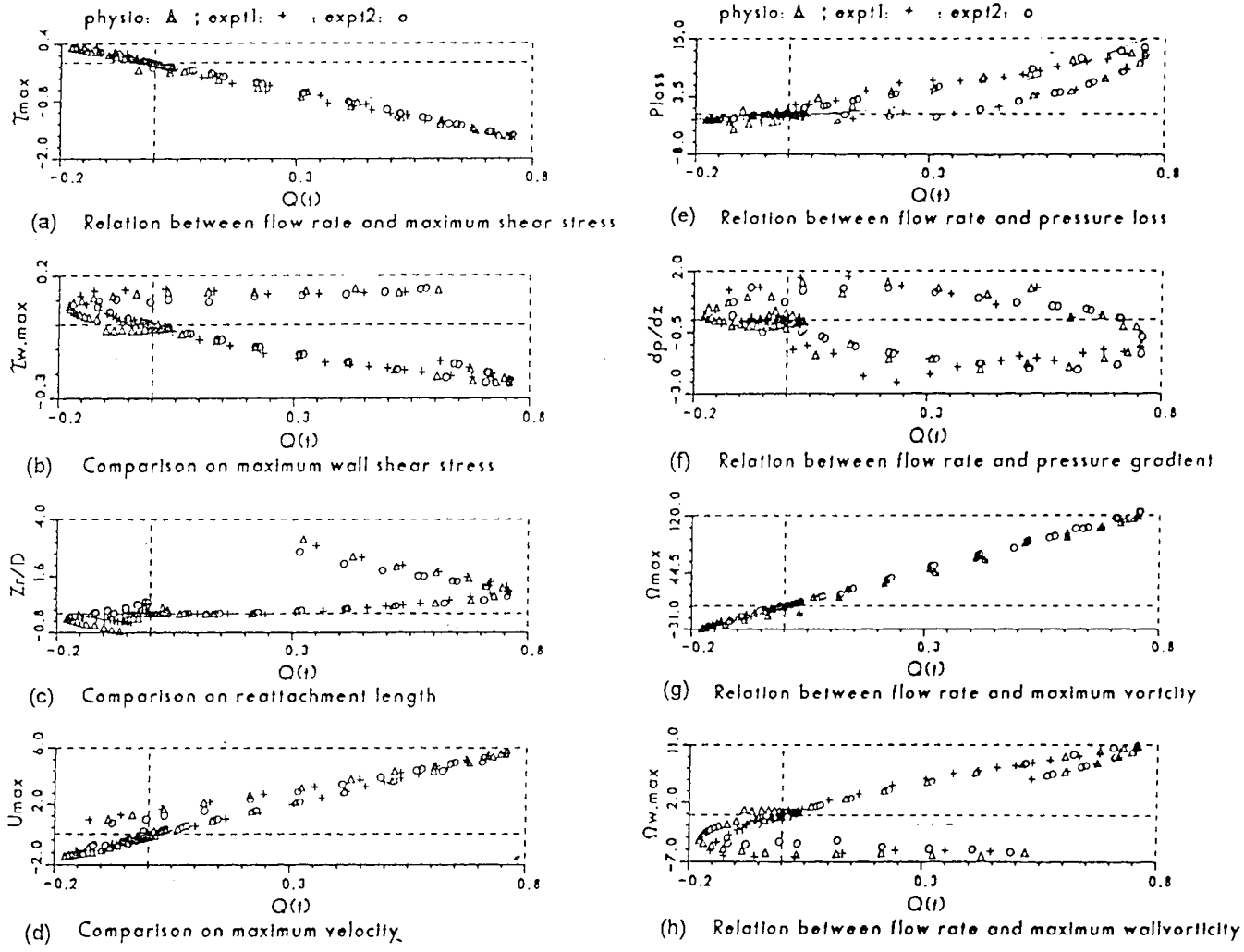

Figure 11. Comparison on three types of pulsatile laminar flows in pipe with a ring-type constriction of $d/D = 0.5$, $h/D = 0.1$ and $Re = 50$, $St = 0.155$.

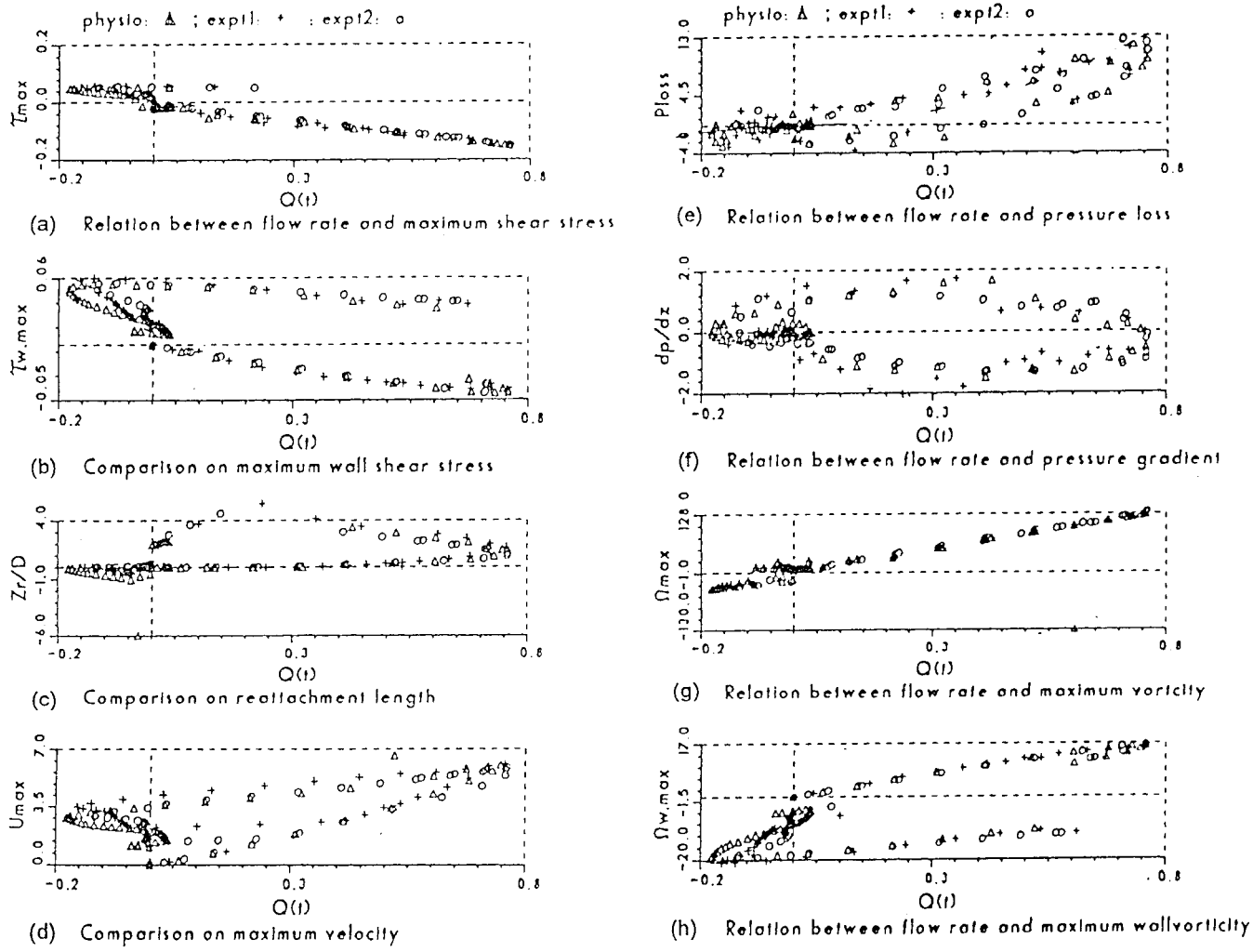

Figure 12. Comparison on three types of pulsatile laminar flows in pipe with a ring-type constriction of $d/D = 0.5$, $h/D = 0.1$ and $Re = 500$, $St = 0.155$.

value in a cycle of the pulsatile flow. Other linear relations exist between the flow rate and the maximum velocity, maximum vorticity and maximum shear stress within the pulsatile flow field.

ACKNOWLEDGMENTS

The authors gratefully acknowledged the contributions of Dr SH Winoto and Mr Ng Tiong Wei in the completion of this work. The support of a National University of Singapore research grant (RP0633) is also gratefully acknowledged. The comments provided by visiting Professor S. Pejovic is also hereby acknowledged.

APPENDIX A. NOMENCLATURE

a	pulsatile amplitude
A	pulsatile amplitude, $A = a/D$
d	orifice diameter
D_1	upstream pipe diameter
D_2	downstream pipe diameter
D	pipe diameter (characteristic length)
$\mathrm{d}p/\mathrm{d}z$	pressure gradient in axial direction
$\overline{\mathrm{d}p/\mathrm{d}z}$	time-averaged pressure gradient, $1/T \int^T \mathrm{d}p/\mathrm{d}z \, \mathrm{d}t$
h	constriction thickness
Nw	Womersley number, $Nw = \sqrt{\omega/v}$
p	pressure
P_{loss}	pressure loss across constriction
ΔP	pressure difference between upstream and downstream flow
$\bar{P}_{\mathrm{loss}}$	time-averaged pressure loss, $1/T \int^T P_{\mathrm{loss}} \, \mathrm{d}t$
Q	flow rate, $Q = Q(t) = (\pi/4)D^2\bar{u}(t)$
$Q_{\max}$	maximum flow rate = 1.0
r	radial co-ordinate, radial distance
Re	Reynolds number, $Re = UD/v$
St	Strouhal number $St = D/(\bar{u}_{\mathrm{peak}})$ or $St = (1/2\pi)(Nw^2/Re)$
t	time co-ordinate, time step
T_{s}	time period of sinusoidal flow
T	time period of physiological flow
u	axial velocity component
$\bar{u}(t)$	instantaneous bulk velocity in pipe
$\bar{u}_{\mathrm{peak}}$	the peak $\bar{u}_{\mathrm{peak}}$ value (characteristic velocity)
U	net forward velocity in a cycle, $U = \int^T Q(t) \, \mathrm{d}t$/(cross section area)
v	radial velocity component
z	axial co-ordinate, axial distance
z_{r}	recirculation length

Greek letters

α_p	underrelaxation factor in updating the pressure
ρ	density of fluid
v	fluid molecular kinetic viscosity

τ shear stress $\tau = (1/Re)((\partial u/\partial r)+(\partial v/\partial z))$
ξ, η co-ordinate variables in general curvature co-ordinate
Ω vorticity, $\Omega = (\partial u/\partial r)-(\partial v/\partial z)$

REFERENCES

1. L.M. Strivastava, 'Flow of couple stress fluid through stenotic blood vessels', *J. Biomech.*, **18**, 479–485 (1985).
2. N. Masahide and S. Tadashi, 'Numerical study on the unsteady flow of non-Newtonian fluid', *ASME J. Biomech. Eng.*, **112**, 100–103 (1990).
3. H. Huang, V.J. Modi, B.R. Seymour and R. Raliga, 'Fluid dynamics of stenosed arteries: a numerical study', *Proc. 6th Int. Conf. on Biomedical Engineering*, 1990, pp. 535–540.
4. Z. Lou and W.J. Yang, 'A computer simulation of the non-Newtonian blood flow at the aortic bifurcation', *J. Biomech.*, **26**, 37–49 (1993).
5. T.S. Lee, 'Numerical studies of fluid flow through tubes with double constrictions', *Int. J. Numer. Methods Fluids*, **11**, 1113–1126 (1990).
6. T.S. Lee, 'Steady laminar fluid flow through variable constrictions in vascular tubes', *J. Fluids Eng. ASME*, **116**, 66–71 (1994).
7. T.S. Lee and H.T. Low, 'Separation and reattachment of fluid flow through series vascular constriction', *J. Finite Elem. Anal. Des.*, **18**, 365–377 (1994).
8. E.H. Jones Jr. and R.A. Bajura, 'A numerical analysis of pulsating laminar flow through a pipe orifice', *ASME J. Fluids Eng.*, **113**, 199–205 (1991).
9. H. Suzuki, Y. Inoue, T. Nishimura, K. Fukutani and K. Suzuki, 'Unsteady flow in a channel obstructed by a square rod (criss-cross motion of vortex)', *Int. J. Heat Fluid Flow*, **14**, 2–9 (1993).
10. D.A. McDonald, 'The relation of unsteady pressure to flow in arteries', *J. Physiol.*, **127**, 533–552 (1955).
11. D.A. Steinman, Vinh Bach, C.R. Ethier, M. Ojha, R.S.C. Cobbold and K.W. Johnston, 'A numerical simulation of flow in a two-dimensional end-to-side anastomosis model', *ASME J. Biomed. Eng.*, **115**, 112–118 (1993).
12. H.W. Sung and A.P. Yoganathan, 'Secondary flow velocity patterns in a pulmonary artery model with varying degrees of valvular pulmonic stenosis: unsteady *in vitro* studies', *ASME J. Biomech. Eng.*, **112**, 88–92 (1990).
13. R. Marcelo, A. Mahamad and C. Ricardo, 'Computation of incompressible turbulent flows by an opposed-differencing scheme', *Numer. Heat Transf.*, **12**, 307–320 (1987).
14. S.V. Patankar, *Numerical Heat Transfer and Fluid Flow*, Hemisphere, Washington, DC, 1980.
15. D.K. Kwon, 'Solution procedure for unsteady two-dimensional boundary layer', *ASME J. Fluids Eng.*, **110**, 334–343 (1984).
16. M. Napolitano and P. Cinnella, 'A numerical study of planar and axially-symmetric sudden expansion flows', *Comput. Fluids*, **17**, 185–193 (1989).
17. A. Pollard, 'A contribution on the effects of inlet conditions when modelling stenosis using sudden expansions', *J. Biomech.*, **14**, 349–355 (1981).
18. D.W. Coder and F.T. Buckley Jr., 'Implicit solutions of the unsteady Navier–Stokes equation for laminar flow through an orifice within a pipe', *Comput. Fluids*, **2**, 295–315 (1974).
19. F. Durst, A.B. Wang and M. Founti, 'Similarity phenomena and computations of the flow through an axisymmetric ring-type obstacle attached to a pipe wall', *Proceedings of Computational Modelling and Experimental Methods in Hydraulics* (HydroComp '89), 1989, pp. 338–350.
20. T.S. Lee, Z.D. Shi and S.H. Winoto, 'Numerical study of transitional turbulent pulsatile flow in pipes with ring-type constrictions', *Int. J. Numer. Methods Fluids*, **22**, 1169–1187 (1996).

